Predicting the therapeutic capabilities of macrophages: Validation of a computational model

Thalia G. Newman

Fall 2022 - Spring 2023

LAFAYETTE COLLEGE

Research Advisor: Robert A. Kurt, Ph.D.

Thesis Committee: Chun Wai Liew, Ph.D., Nancy Waters, Ph.D.

Table of Contents

Biographical Sketch

In my sophomore year of high school, I suffered a grade 2 concussion that severely impacted my ability to read, write, and generally succeed in my classes. For nearly six months, I struggled to study for more than an hour at a time without a debilitating headache. Yet, whenever I felt up to it, I always found myself coming back to biology. As I continued taking more science courses over the next few years, my love for the subject grew and I eventually chose to continue my studies as a biology major at Lafayette College.

I began my journey at Lafayette with a general interest in biology and human medicine, but without any knowledge of specific fields or career paths that interested me. So, I took every opportunity I could to learn more. I took courses in statistics, biomedical informatics, and genetics. However, it wasn't until the fall semester of my junior year that something truly stood out to me. When I took immunology last fall, it was by far the hardest class I had ever taken. I had never encountered a subject that involved so many systems existing independently while still working in tandem with each other, covering diverse mechanisms, concepts, and conditions. Despite the challenges of the course, I found myself driven to return to the material and learn more. I spent hours studying, scribbling diagrams of T cell activation mechanisms, and creating numerous flashcard decks to help myself understand the concepts being presented. That same semester, I began work as an independent research student under Dr. Kurt, using a computational approach to study interactions between the TLR4 and TLR5 signaling pathways. This work, in tandem with the immunology course I was taking, made it clear to me that immunology was a subject that I genuinely enjoyed learning about. I knew that I wanted to be at the forefront of new immunological discoveries through a career in immunology research, and I chose to pursue a senior honors thesis.

The following summer, with the background I had from my courses and research experience, I was fortunate to participate in an internship at the Benaroya Research Institute in Seattle, Washington, a distinguished research facility that focuses on the study of immune-mediated diseases. This experience provided me with the opportunity to strengthen my laboratory techniques and developed my understanding of current immunological research.

When I returned to Lafayette for the fall semester, I began designing and working on my honors thesis, expanding upon the work I had conducted as a junior. This experience has been invaluable in my development as a student and a scientist, and it would have been impossible without the support and guidance of Dr. Kurt. I will be graduating this May with a B.S. in Biology, and in August I will begin the pursuit of a Ph.D. through the University of Michigan's Program in Biomedical Sciences, entering with a primary interest in Immunology.

Abstract

This project aimed to alter a computational model of monocyte activation via the Toll-like receptor (TLR) 4 and 5 signaling cascades to provide insights into the pro-inflammatory activation of bone marrow-derived macrophages (BMDM) and to further utilize these findings to enable the prediction of BMDM therapeutic efficacy following TLR stimulation. I aimed to quantify IL-1β produced by BMDM stimulated with varying concentrations of TLR agonists to verify if the computational model could predict the optimal agonist combinations for BMDM activation and to determine if the computational model's predicted activation correlated with therapeutic efficacy. Through an analysis of TLR-related gene expression in both monocytes and BMDM, I identified one gene expressed at a higher level and three genes expressed at lower levels in BMDM relative to monocytes. I then incorporated these differences in gene expression into the modeling parameters, to observe the model's ability to predict cell activity. Experimentally, production of the pro-inflammatory cytokine IL-1β generally increased as TLR agonist concentration increased, and IL-1β production peaked and stabilized 24 hours post-treatment. BMDM treated with high concentrations of TLR4 and TLR5 agonists were able to temporarily delay tumor growth compared to BMDM treated with HBSS. Medium agonist concentrations contributed to the development of more aggressive tumors, and low concentrations of agonists provided a sustained benefit in delaying tumor growth and severity. While the model's misalignment with experimental results suggested that a different approach may benefit model adaptation, therapeutic tests did reveal that polarization toward a pro-inflammatory state, defined by produced IL-1β, had significant effects on both tumor growth and severity. This highlighted that the concentration of agonists used for cell stimulation is critical in predicting the therapeutic efficacy of BMDM as a potential tumor therapy.

Introduction

The innate immune system, comprised of physical and anatomical barriers, effector cells, antimicrobial peptides, soluble mediators, and cell receptors is crucial for its role as the first line of defense against pathogens encountered by an individual. The components of this system work in combination to recognize and initiate responses to foreign substances that enter the body, dispelling many potentially harmful substances and protecting an individual from illness (Aristizábal, 2013). Macrophages, a type of innate phagocytic effector cell, have reported functions in development, homeostasis, tissue repair, and immunity (Wynn, Chawla, & Pollard, 2013), making them one of the most involved cells of the innate immune system. Postnatal macrophage development occurs through the differentiation of circulating monocytes, and the activation and further differentiation of these monocytes can be polarized towards the inflammatory M1 macrophage phenotype or the anti-inflammatory M2 phenotype through exposure to specific environmental factors which trigger responses through TLRs.

TLRs are a type of pattern recognition receptor (PRR) that exist both intra- and extracellularly as a part of circulating monocytes to detect and initiate responses to unique pathogen-associated molecular patterns (PAMPs) (Kawasaki & Kawai, 2014). Upon recognizing its specific pattern, certain TLRs, including TLRs 4 and 5, initiate a signaling pathway that contributes to cell activation and differentiation into an M1 macrophage, which then goes on to function as a pro-inflammatory cell in the affected tissue (Juhas et al., 2015).

M1 macrophages have also been shown to have anti-tumor capabilities. Through their secretion of cytokines TNFα, IL1β, and IL12 and chemokines CXCL9 and CXCL10, they promote a Th1 response, which furthers inflammatory responses at affected sites to enhance the

recruitment of other immune cells (van Dalen et al., 2019). M1 macrophages are also known to upregulate genes involved in antigen processing and presentation, improving T-cell responses (Martinez & Gordon, 2014). When these macrophages are exposed to tumor cells, their enhancement of the inflammatory process results in improved recruitment of other immune cells which can then work to eliminate cancer cells. Translating this characteristic into therapy, studies done as early as the 1980s have examined how the injection of laboratory-derived M1 macrophages, induced from monocyte-derived macrophages stimulated with IFNγ, affects tumor development (Andreesen et al., 1990). These cells, coined as macrophage-activated killer (MAK) cells, have demonstrated some ability to slow tumor progression when injected into cancer patients with little to no side effects, but additional studies are needed to ensure that MAK cells aren't reverting to an M2 tumor-associated macrophage (TAM) phenotype when exposed to the tumor microenvironment (TME) and to improve upon clinical results (Anderson et al., 2021).

To accelerate the process of determining the best way to generate MAK cells for tumor therapies, one can turn to a model. Models, whether they are mathematical or computational, have long been used to facilitate the testing of multi-variate experiments, as they, once calibrated to ensure they resemble results shown experimentally, can provide a glimpse into the behavior of variables of interest for a fraction of the cost and time that would otherwise go towards experimental testing. Previously, a computational model was created simulating the activation of monocytes when exposed to TLR stimuli (Liew et al., 2018). This project examined whether this pre-existing verified model was also applicable to BMDM. As BMDM are derived from monocytes, they share many characteristics, and it would be reasonable to assume that they may behave similarly to the same stimuli. This project focused on validating this claim, verifying that the model was applicable to BMDM and testing if levels of activation of BMDM affected their

therapeutic capabilities. Future directions for the verified model include its direct application to research that aims to study MAK cells as tumor therapies, streamlining the research process to predict TLR agonist combinations that are the most effective in tumor treatment without spending absorbent amounts of time or money on experimental tests of the same conditions.

To examine whether the pre-existing computational model could be applied to the prediction of M1 BMDM responses, I performed an initial analysis of modeling data to predict levels of the TLR4 and TLR5 agonists lipopolysaccharide (LPS) and flagellin (FLA) that should be used to generate high, medium, and low levels of activation from monocytes. To modify the model for BMDM, I used RT-qPCR to determine the expression of TLR signaling-related genes in BMDM relative to those of monocytes. I then stimulated BMDM with the model-predicted agonist combinations, and measured activation and polarization towards the M1 phenotype through an ELISA quantifying IL-1β production, one of the cytokines associated with M1 phenotypic macrophages, to determine if BMDM activation mirrors that of monocytes. This demonstrated the ability of the model to predict the activation level of BMDM in response to TLR agonist stimulation. To test whether these activation levels affected BMDM therapeutic efficacy, an EMT6 murine mammary carcinoma model was utilized to examine how MAKs derived from BMDM at low, medium, and high levels of activation affected tumor growth and development.

I hypothesized that the model would be applicable to the BMDM due to the shared morphological similarities and TLR pathway functions between BMDM and monocytes. I also hypothesized that highly activated BMDM would display the best therapeutic results due to their increased cytokine production, allowing them to recruit a greater abundance of other immune cells to the tumor site.

Materials & Methods

Computational Modeling

Computer simulations were run in a previously constructed TLR4 and TLR5 dual signaling model that was written in Scala (version 2.13.3) and runs on the Ubuntu (20.04) operating system, with executable NetLogo programs generated for the NetLogo 6.0.1 environment. Parameters included (and values in the initial THP-1 model) were number-tab3d (0), number-ikk-complex (50), number-deactivated-tak1 (50), number-nfkb (50), number-activated-tak1(0), number-tlr4 (25), number-tab2 (50), number-tab1 (50), number-ikba (0), number-traf6 (0), number-lps (varied), number-tab4d (0), number-dna (10), number-fla (varied), number-irak4 (50), number-tab3 (50), number-irak2 (100), number-tlr5 (25), number-ubc13 (50), number-rna (0), number-tab1d (0), number-irak-m (75), number-foo1 (0), number-nfkb_n (0), number-tab2d (0), number-rna-c (0), number-irak1 (100), number-myd88 (250), membrane-ycor (21), nucwall-ycor (-17), delta-movement (0.5), tick-delta (200), and decay-time (500). Outputs were given as count tab4ds, count rnas, count tab3ds, count tab2ds, count foo1s, count traf6s, count tab1ds, count activated-tak1s, and count ikbas. For the purposes of this project, number-nfkb, number-tlr4, number-tab2, number-tab1, number-lps, number-fla, number-irak4, number-tab3, number-irak2, number-tlr5, number-irak1, and number-myd88 were studied, and count-rnas was measured as the output variable of interest.

Modeling Analysis

Data were uploaded into Posit Cloud and reformatted to be readable and to stack all runs analyzing the variable(s) of interest. Files were analyzed in Posit directly, or exported as new CSV files and opened and analyzed using google sheets. LPS and FLA amounts were grouped

into “low” (5, 10, 25), “medium” (50, 100, 250), and “high” (500, 1000, 2500) categories to better view general trends in RNA output as a result of agonist level changes. At each timestep, RNA output was summed with output from preceding timesteps, to capture the cumulative output over time and reflect the long-term stability of proteins tested experimentally when incubated at 37℃.

THP-1 Maintenance

The THP-1 cell line used for experimental testing of aim one was purchased from InvivoGen (San Diego, CA), and aliquots of the cell line were stored in liquid N_2. Prior to experiments, THP-1 cells were thawed and maintained in 25cm^2 culture flasks with 5ml cRPMI (Corning 1x RPMI 1640 with L-glutamine supplemented with 10% heat-inactivated Neuromics fetal bovine serum, 2mM Lonza BioWhittaker® L-glutamine, 100 U/mL Lonza Biowhittaker® penicillin/streptomycin, 1x Lonza Biowhittaker® NEAA Mixture, 5x10-5 M Sigma-Aldrich 2-mercaptoethanol, and 1mM Lonza Biowhittaker® sodium pyruvate) at 37°C with 5% CO_2. Cells were split three times per week.

THP-1 TLR Agonist Treatment

THP-1 cells were adjusted to a concentration of 5.6 x 10^5 cells/mL and 180 µL of cells were added to wells of a 96-well round-bottom plate. To assess the interactions between TLR signaling pathways, cells were treated with 50 µl of 1X gibco HBSS, 0.05 µg/mL LPS diluted from InvivoGen 5 mg stock, 0.5 µg/mL LPS, or 5 µg/mL LPS, in combination with 50 µl of HBSS, 0.05 µg/mL FLA diluted from InvivoGen 100 µg stock, 0.5 µg/mL FLA, or 5 µg/mL FLA. Cells were incubated with the agonists at 37°C with 5% CO_2 for 2, 6, 12, 24, or 72 hours prior to analysis.

THP-1 Agonist Response Analysis

Cell supernatants were collected 2, 6, 12, 24, or 72 hours after agonist treatment and were transferred to a new 96-well flat-bottom plate containing 180 µL prepared InvivoGen QUANTI-Blue™ solution. The plate was incubated for 1 hour at 37℃, 5% CO_2 before optical density was read at 650 nm using an Infinite® 200 PRO Tecan microplate reader.

Mice Breeding & Care

BALB/c mice were bred on-site and housed in a Thoren caging system with *ad libitum-provided* food and water and were utilized in accordance with the Institutional Animal Care and Use Committee (IACUC) guidelines for ethical conduct in the care and use of animals.

BMDM Culture Preparation

BALB/c mice were humanely euthanized through exposure to CO_2 gas followed by cervical dislocation. Mice were skinned from the waist down, and legs were removed from the body at the hip joint. Bones were cleaned of excess tissue and were added to petri dishes with 5 mL cRPMI. Bone marrow was collected from the hind legs using a BD 25G x ⅝ 1 mL TB syringe to push 0.5-1.0 mL of cRPMI through both the femur and the tibia at least three times, alternating the end of the bone at which the needle was inserted. Ten additional mL cRPMI was added to the petri dish, and the total 15 mL cRPMI containing bone marrow was passed through a Falcon® 40 µm nylon cell strainer into a Falcon 50 mL tube. Cell strainer was rinsed with an additional 10 mL of cRPMI, bringing the total volume to 25 mL. The cells were spun down at 400 xg for 8 minutes, supernatant was discarded, and precipitate was dislodged by manually flicking the tube. Five mL red blood cell lysis buffer (1 L H_2O, 8.29 g NH_4Cl, 1.0 g $KHCO_3$, 37.2 mg EDTA, pH adjusted to 7.2) and 5 mL cRPMI was added before the cells were spun down at

400 xg for 8 minutes to facilitate the removal of red blood cells. Supernatant was poured off, and the bone marrow mononuclear cells (MNCs) were resuspended in 25 mL cRPMI containing 10 ng/mL macrophage colony-stimulating factor (M-CSF) diluted from Peprotec 10 µg stock to encourage macrophage development. Cells were transferred in 1 mL aliquots across 24-well cell culture plates, and media was replaced with fresh cRPMI supplemented with M-CSF every two to three days for one week for use on the seventh day.

Primer Preparation

The National Center for Biotechnology Information's RefSeq database was utilized to identify reference sequences for both human and mouse *Gapdh*, *Tlr4*, *Tlr5*, *RelA*, *Myd88*, *Irak1*, *Irak2*, *Irak4*, *Tab1*, *Tab2*, *Tab3*. Primer3 v. 0.4.0 was used to identify potential primers for each sequence. Amplicon length was set to 75-150 bp, optimal melting temperature was set to 68°C, and the range for GC content was set from 50-60%. Preference was given to primers that had no GC stretches longer than 3 bp in length, no Gs at the 5' end, no more than 2 Gs or Cs in the last 5 spots at the 3' end, and no 3' complementarity. Forward and reverse primer sequences were run through the nucleotide BLAST local alignment search tool to confirm specificity and were ordered as 25 nmole DNA oligos from Integrated DNA Technologies. Purchased primers were reconstituted with 1 mL Sigma-Aldrich PCR-grade water. To prepare primer stock solutions, 30,000 was divided over the primer-specific OD_{260} value times 33 to determine the volume of primer added in µL. Calculated volumes of forward and reverse primers were combined, and PCR-grade water was added to bring the stock volume to 1 mL.

TLR Gene Expression Quantification

RNA was collected from untreated THP-1 cells and cultured BMDM utilizing the BioRad Aurum™ Total RNA Mini Kit. To create cDNA from collected RNA, 15 µL RNA was combined with 4 µL BioRad 5x iScript Reaction Mix and 1 µL BioRad iScript Reverse Transcriptase and placed in an MJ Research MiniCycler™ to run on a pre-set cDNA cycle (25.0°C for 5 minutes, 46.0°C for 20 minutes, 95.0°C for 1 minute, hold at 4.0°C for up to 24 hours). For each PCR reaction, 4.5 µL PCR-grade water, 0.5 µL cDNA, 12 µL BioRad iTaq Universal SYBR® Green Supermix, and 7.5 µL of a prepared primer stock solution were added to a well of a BioRad PCR plate. The BioRad CFX Connect real-time PCR detection system was used in data collection. Data were returned in CFX Manager.

Analysis of RT-qPCR

GAPDH was set as the reference gene for expression analysis. For each of the three experiments, BMDM expression was compared against THP-1 expression, setting THP-1 expression to 1. Data were organized in google sheets, and relative expression in BMDM for each of the three experiments was averaged to produce a summary figure, constructed in Posit Cloud. Standard errors were calculated and included as error bars.

BMDM TLR Agonist Treatment

To treat BMDM, 50 µl of HBSS, 0.05 µg/mL LPS, 0.50 µg/mL LPS, or 5.00 µg/mL LPS was added to each well of the 24-well cell culture plate utilized to culture BMDM, alone or in combination with 50 µl 0.05 µg/mL FLA, 0.50 µg/mL FLA, or 5.00 µg/mL FLA. Cells were incubated with the agonists at 37°C with 5% CO_2 for 2, 6, 12, 24, 48, or 72 hours prior to collection. BMDM supernatants (600 µL) from wells of stimulated cells were collected 2, 6, 12, 24, 48, or 72 hours following agonist treatment and were kept at -20℃ until analysis

BMDM Agonist Response Analysis

Analysis was performed with the R&D Systems Quantikine™ ELISA kit specific for either mouse IL-1β or mouse TNF-α. Each sample was run in duplicate, with 3 repeats of the experiment. Data were collected by reading optical density at 450 nm using an Infinite® 200 PRO Tecan microplate reader with 16 reads per well and at 570 nm with one read per well. Data was returned in an Excel spreadsheet.

Analysis of ELISA Data

Data were collected in google sheets. The reads at 450 were averaged, and the read at 570 was subtracted from this average as correction. The read produced by the negative control (assay diluent only, no IL-1β/TNF-α) was further subtracted from each well. A linear regression of reads from the protein standard solutions (included with the R&D Systems Quantikine™ ELISA kit) was used to calculate the concentration of IL-1β/TNF-α present in each well in pg/mL. Standard errors were calculated for each treatment condition and were added to plots as error bars. Data were transferred into Posit Cloud for construction of visual representations of data.

EMT6 Maintenance

EMT6 cells were thawed from liquid N_2 stocks and were incubated at 37℃ and 5% CO_2, maintained in cRPMI, and split three times per week.

BMDM Preparation for Therapeutic Testing

BMDM were cultured and divided into four treatment conditions to produce cells activated at high, medium, and low levels in addition to untreated BMDM serving as a control cell population. Highly activated BMDM were treated with 10 μL 5.00 μg/mL LPS and 10 μL

5.00 µg/mL FLA. BMDM activated at a medium level were treated with 10 µL 0.50 µg/mL LPS and 10 µL 0.50 µg/mL FLA. BMDM activated at a low level were activated with 10 µL 0.05 µg/mL LPS and 10 µL 0.05 µg/mL FLA. Control BMDM were not treated with TLR agonists and instead had 20 µL HBSS added to each well. Cells were incubated at 37°C with 5% CO_2 for 24 hours prior to collection.

BMDM Collection

Media was collected from treated BMDM. Wells were washed with approximately 0.5 mL HBSS, which was added to collected media. Next, 100 µL of 1x PBS 10 mM EDTA was added to each well, and the plate was placed on ice for 5 minutes. The collected media (700 µL) was used to pipet up and down in each well to dislodge BMDM. All remaining media was collected from the well. If BMDM were to be injected in combination with EMT6 cells, cell concentrations were adjusted to be equivalent before cell types were combined. Cells were then spun down at 400 xg for 8 minutes, washed three times with 10 mL HBSS, and adjusted to a concentration of $1x10^6$ BMDM per mL suspended in HBSS. If BMDM were to be injected alone, cells were spun down at 400 xg for 8 minutes, washed three times with 10 mL HBSS, and adjusted to a concentration of $1x10^6$ cells per mL suspended in HBSS.

EMT6 Collection

Media was collected and discarded from the flask containing EMT6 cells. The cells were washed with 5 mL HBSS, which was then discarded. One mL of Gibco 0.25% Trypsin-EDTA (1X) was added to the flask, which was incubated at 37°C with 5% CO_2 for 5 minutes before 9 mL of cRPMI was added and cells were dislodged by tapping the flask against a hard surface. Media was collected and cells were counted. If EMT6 were to be injected in combination with

BMDM, cell concentrations were adjusted to be equivalent before cell types were combined. Cells were then spun down at 400 xg for 8 minutes, washed three times with 10 mL HBSS, and adjusted to a concentration of $1x10^6$ EMT6 cells per mL suspended in HBSS. If EMT6 were to be injected alone, cells were spun down at 400 xg for 8 minutes, washed three times with 10 mL HBSS, and adjusted to a concentration of $1x10^6$ cells per mL suspended in HBSS.

Determination of Therapeutic Capabilities

BALB/c mice were subcutaneously injected with 100 µL of cell solution. In group A, 24 mice made up four treatment groups with 6 mice per group, and received an injection of EMT6 cells combined with BMDM that had been treated with 5.00 µg/mL LPS and 5.00 µg/mL FLA, 0.50 µg/mL LPS and 0.50 µg/mL FLA, 0.05 µg/mL LPS and 0.05 µg/mL FLA, or HBSS alone. An additional 24 mice made up 4 treatment groups in group B with 6 mice per group, with each mouse receiving an injection of EMT6 cells one week prior to an injection of BMDM that had been treated with 5.00 µg/mL LPS and 5.00 µg/mL FLA, 0.50 µg/mL LPS and 0.50 µg/mL FLA, 0.05 µg/mL LPS and 0.05 µg/mL FLA, or HBSS alone. After day 7, tumor size was measured every 2-3 days following injection until day 28 or until tumor size exceeded 1500 mm^3, and the mice were then sacrificed. Experiments were repeated at least two times.

Analysis of Tumor Sizes

A caliper was used to measure the length (longer measurement) and width (shorter measurement) of the size of subcutaneous tumors in mm. The equation $\frac{length \bullet width^2}{2}$ was used to find the volume of each tumor in mm^3. Data was collected in Google Sheets and exported into Posit Cloud. Tumor volumes from each treatment condition were averaged. Standard errors were calculated and included in figures as error bars. Once one mouse from a treatment group had

died, exponential regression was performed on data collected thus far from that treatment group, to approximate the treatment group's average tumor size at subsequent checkpoints to allow for an extended comparison to other treatments. Mice that did not develop a palpable tumor at any point during the 28-day period were excluded from analysis.

Statistical Analysis

In analyses of BMDM IL-1β production and tumor sizes, Bonferroni corrections were used to establish the p-values corresponding to confidence levels of 95%, 99%, and 99.9% based on the number of comparisons being performed. After normality was assessed using a Shapiro-Wilks test and histogram generation, unpaired, one-tailed Welch's two-sample t-tests were used to determine the significance of differences that were observed between samples. In analyzing survival probability over time, the probability of survival was calculated by dividing the mice from a treatment group living on a given day by the number of mice in that treatment group at day 0. After performing a Bonferroni correction to establish p-values corresponding to confidence levels of 95%, 99%, and 99.9%, log-rank tests were used to estimate the significance of differences in overall survival probability observed between the control group and each treatment group.

Results

TLR-related gene expression differs between THP-1 cells and BMDM

RT-qPCR data revealed significant differences between BMDM and THP-1 cells in the expression of *Irak1*, *Irak2*, *RelA*, and *Tab3* (Fig. 1). *Irak1* and *RelA* were expressed at a ratio of almost 0:1 (Table 1). *Irak2* expression was noticeably increased in BMDM, with an expression level approximately 70 times that of THP-1 cells (Table 1). Expression levels of *Irak4*, *Tab1*, *Tab2*, *Tlr4*, and *Tlr5* in BMDM seemed to show variation from THP-1 cells, but there was not sufficient evidence to indicate a true difference in mean expression at a 95% confidence level due to variability in the data.

Modeling efforts are successful in producing consistent patterns of RNA output in response to varying LPS and FLA levels

From the RT-qPCR data (Fig. 1), baseline values in the model were adjusted: IRAK1, TAB2, TAB3, and TLR5. IRAK2 was not modified despite the dramatic increase in expression shown in BMDM, as it was already present in excess in the model, and it was not believed that increasing its quantity would have an effect on the simulation. NFκB, the modeling equivalent to the tested murine RELA, was unable to be adjusted without inhibiting model function and was also left unchanged. IRAK1 was decreased from 100 to 25, TAB3 from 50 to 25, TLR5 from 25 to 5, and TAB2 was increased from 50 to 100 for round 1 of the model (Table 1).

The first round of modeling incorporating these parameters showed some response to LPS variation and appeared to reveal a dose-dependent pattern when averaged (Figs. 2a-b), but inconsistencies were seen when separating the data from the grouped “high”, “medium”, and “low” LPS levels. Increasing LPS by a factor of 10, corresponding with the increases in

experimental concentrations of 0.05 μg/mL, 0.50 μg/mL, and 5.00 μg/mL LPS, had inconsistent effects on cumulative RNA output. Increasing LPS from 10 to 100 showed an initial increase, but there was no increase when LPS was further increased to 1000 (Fig. 2c). An increase in LPS from 25 to 250 significantly increased the RNA output, hitting the peak production point, yet this output dropped back down when LPS was increased to 2500 (Fig. 2c). Comparing LPS 50 to LPS 500, LPS 500 produced values that were slightly lower than LPS 50 (Fig. 2c). When considering all values in succession, a significant increase in total RNA output was seen as LPS was increased from 10 to 250, but output dropped when it reached 500, before increasing again when LPS was increased to 1000 and 2500 (Fig. 2c). In summary, the first round of modeling data showed a dose dependent pattern when runs were grouped into high, medium and low LPS levels. However, when considering individual levels of LPS, there was no trend in how LPS levels affected RNA output.

In an effort to achieve a model that would show a dose dependent response to individual doses of LPS, a second round of modeling was conducted with IRAK1 increased from 25 to 30, shifting closer to the original value seen in the functional THP-1 model. With this modification, results were similar to those observed with the round 1 model. When the data were grouped, a dose dependent response was evident (Figs. 2d-e). However, inconsistencies were seen when individual doses of LPS runs were compared. For instance, setting LPS at 100 and 1000 produced the same level of RNA output (Fig. 2f). Increasing LPS from 25 to 250 resulted in a decrease in RNA output (Fig. 2f), and increasing LPS from 50 to 500 produced a slight decrease (Fig. 2f). Due to the lack of a dose dependent response, the model was adapted again.

For the third round of modeling, IRAK1 was returned to 25 and TAB2 was dropped to 50, because further analysis of the initial RT-qPCR results revealed that the increase in TAB2

expression in BMDM relative to THP-1 cells was not statistically significant. With these adjustments to the model, RNA output values were found to be consistently lower than they had been in previous runs. When the data were grouped, the low and high LPS groups each resulted in higher levels of RNA output than the medium group (Figs. g-h). When looking at the data from individual doses, inconsistencies in RNA output were more apparent than in previous rounds of modeling. Notably, setting LPS at 250 produced no response (Fig. 2i). LPS 25 and 2500 produced the same level of RNA output, as did LPS 50 and 500. Thus, round 3 of the model displayed even less evidence of a dose-dependent response than rounds 1 or 2 of the model.

Each of the models thus far had relied on rounded input values derived from the RT-qPCR ratios, and as no dose dependent effect was seen, the fourth round of modeling aimed to match the RT-qPCR ratio-derived values as close as possible, rounding to the nearest whole number as opposed to the nearest multiple of 5 or 10. This fourth round was also the first to incorporate FLA to observe the interaction between the two signaling pathways. Results from round 4 of the model revealed that FLA consistently increased RNA output beyond what was produced from runs with LPS alone (Fig. 3). It appeared that combinations of low and medium FLA with LPS produced a relatively consistent effect, with low LPS/low FLA and medium LPS/low FLA producing similar results (Fig. 3a). Runs examining low LPS/medium FLA and medium LPS/medium FLA also mirrored eachother (Fig. 3a). When low or medium FLA were combined with high LPS, the total RNA output decreased slightly but still displayed similar patterns (Fig. 3a). In contrast, high FLA produced a consistently high RNA output when combined with either medium or high levels of LPS, but produced relatively low levels of RNA

when combined with low LPS (Figs. 3a-c). Additionally, model 4 displayed more stability with respect to a dose dependent effect (Fig. 3d) than observed with models 1-3.

Collectively, these data show that using the RT-qPCR-derived information about differences in TLR-associated gene expression between BMDM and THP-1 was able to achieve a consistent pattern of RNA output with different levels of LPS and FLA, indicating that the model was able to generate a dose dependent response to LPS and FLA.

TLR stimulation increases expression of IL-1β and TNF-α in BMDM

The ELISA analysis of cultured BMDM treated with LPS reflected a sharp increase in IL-1β concentration when cells were treated with 5 μg/mL LPS, compared to 0.05 or 0.50 μg/mL LPS which produced no notable difference (Fig. 4a). At 24, 48, and 72 hours, the length of time since treatment did not have a significant effect on protein production. As there was no change in IL-1β production after the 24 hour timepoint, additional tests were performed on BMDM incubated with agonists for 2, 6, and 12 hours, excluding the 0.05 μg/mL LPS treatment due to it's similarity to the 0.50 μg/mL LPS treatment. IL-1β produced by BMDM stimulated with 0.50 μg/mL and 5.00 μg/mL LPS rose steadily for the first six hours following incubation (Fig. 4b). By 12 hours, the IL-1β produced by cells treated with 0.50 μg/mL LPS had peaked and remained consistent at future timepoints, while the IL-1β production by cells treated with 5.00 μg/mL LPS rapidly increased, stabilizing at 24 hours post-treatment (Fig. 4b).

Simultaneous treatments of cells with LPS and FLA revealed that when cells were stimulated with 0.05 μg/mL or 0.50 μg/mL LPS, all concentrations of FLA contributed to an increase in IL-1β production from that which was seen in cells treated with LPS alone (Fig. 4c). In cells treated with 5.00 μg/mL LPS, the addition of 0.50 μg/mL FLA produced a significantly lower level of IL-1β than the addition of either of the more extreme FLA concentrations (Fig.

4c). Cells stimulated with 5.00 μg/mL FLA consistently produced the greatest amount of IL-1β relative to all other FLA concentrations, regardless of the LPS concentration used in combination. Combining 5.00 μg/mL and 5.00 μg/mL LPS for treatment led cells to produce the most IL-1β overall (Fig. 4c).

Testing for TNF-α production in dual-stimulated BMDM revealed that unlike IL-1β production, TNF-α was not produced in a dose dependent manner. BMDM treated with HBSS alone produced very little TNF-α, while any stimulation of TLR4 alone or in combination with stimulation of TLR5 produced approximately 540 pg/mL TNF-α (Fig. 4d).

ELISA analyses of stimulated cells revealed that all cells peaked in cytokine production by 24 hours post-agonist treatment. Differences between IL-1β and TNF-α production patterns revealed that levels of pro-inflammatory cytokines are produced independently, and may differ in their responses to agonist stimulation.

Agonist treatments have mixed effects on tumor growth

When BMDM and EMT6 were injected simultaneously, mice from the high treatment group (5.00 μg/mL LPS and 5.00 μg/mL FLA) initially showed a statistically significant decrease in tumor size from the control group (Fig. 6a). However, this effect appeared to fade overtime, with the growth rate for the high treatment group rising overtime (Fig. 6a). By day 28, 33% of mice from this group had developed tumors that surpassed 1500 mm^3 (Fig. 6b). Mice from the medium treatment group also showed a lower tumor size than the control group initially, but they quickly developed tumors that were more aggressive than those associated with the control group (Fig. 6a). These mice were the first to begin developing tumors that had surpassed 1500 mm^3 in volume and had to be sacrificed; by day 28 37.5% of mice remained (Fig. 6b). Mice from the low-treatment group initially developed tumors that grew at rates similar to

those of the control group, but by day 28, these mice had a 38% chance of survival, which was better than that of any other treatment group, while mice from the control group had only a 12.5% chance of survival (Fig. 6b).

Considering the delayed injection of BMDM seven days post-EMT6 injection, BMDM treated with high or low agonist concentrations were effective at slowing tumor growth to cause tumor sizes that were significantly lower than those of the control group ($p=0.0255$ and $p=0.0285$) within 5 days of their injection (Figs. 6a-b). These differences remained through day 15, and the high and low treatment groups generally performed similaraly over the course of the 28 day period. By day 22, three mice from the low treatment group no longer had a palpable tumor (Figs. 6a-b).

While mortality trends had appeared similar in mice injected simultaneously regardless of BMDM activation level, when injected at a delayed date mice from the medium treatment group had a lower chance of survival overtime. These mice were the first to develop tumors that had surpassed a volume of 1500 mm^3, and by day 26 only 30% of these mice remained compared to 60% of mice from the high treatment group, 55% from the low treatment group, and 33% from the control group (Fig. 7c).

When comparing the simultaneous tumor and BMDM injections with the delayed BMDM injections, BMDM activated at a high or low level were generally able to best control tumor growth when injected 7 days post-EMT6 injection, rather than with EMT6 (Fig. 8). The simultaneously-injected medium group grew tumors smaller in size than those that were injected at a delayed time, but these mice had a decreased probability of survival long-term, which limited analysis of long-term behavior (Fig. 8). There was no significant difference in tumor growth overtime between the delayed and simultaneous control groups (Fig. 8).

In summary, agonist treatments appeared to have a significant effect on the efficacy of BMDM in slowing tumor growth and limiting tumor severity. In both simultaneous and delayed treatments, BMDM stimulated with high concentrations of LPS and FLA temporarily slowed tumor growth, but had little effect on long-term tumor size or survival. BMDM treated with medium concentrations of LPS and FLA led mice to develop tumors that were more aggressive than those developed by mice treated with control BMDM. And lastly, BMDM that were treated with low concentrations of LPS and FLA were effective in slowing tumor growth over an extended period of time.

Discussion

M1 macrophages have long been studied as a potential tumor therapy, but no previous research has analyzed how the intensity of polarization toward the M1 phenotype may affect the role of macrophages within the TME. Through this study, I attempted to adjust a pre-established computational model of pro-inflammatory monocyte activation to be used for the prediction of M1 polarization intensity following stimulation with varying concentrations of TLR4 and TLR5 agonists, and to further understand how this polarization intensity contributed to the therapeutic efficacy of M1 macrophages.

RT-qPCR revealed notable differences in levels of expression of TLR-associated genes when comparing BMDM to THP-1 monocytes. Accounting for the limitations of the model, adjusting modeling input values to reflect differences in TLR gene expression produced a model that was successful in producing an agonist-dose-dependent pattern of RNA output. This stability provided evidence that the model had the potential to be adjusted for predicting the activation intensity of M1 macrophages. Variations in RNA output following changes of LPS and FLA levels indicated that the stimulation of the TLR5 pathway, with any amount of FLA, contributed to an increase in cell activity beyond that of runs that only considered LPS. RNA output from runs incorporating no, low or medium levels of FLA reflected consistent levels of or decreases in output as LPS level increased, yet an opposite trend was observed when high FLA levels were incorporated into the model, with RNA output increasing as LPS levels increased from low to high. At lower FLA levels, the increases in LPS may have contributed to an overcrowding of the few TLR5 receptors that were present, restricting the receptors from recognizing and binding to FLA as efficiently to initiate signaling, contributing to the decreases in cell activity seen when LPS was increased from low to high levels. These decreases could have also been a result of the

decreased IRAK1 level, which was set to approximately ¼ of the value from the original THP-1 model. The stimulation of the cell with LPS would have triggered the initiation of the TLR4 signaling cascade, recruiting available MYD88. MYD88 would then recruit IRAK to the complex, but the limited IRAK 1 amount would prohibit further pathway completion until the IRAK 1 was available again. This may also have contributed to the slower, progressive build up of RNA overtime, as opposed to the quicker peaks and stabilization observed with the monocyte model. This gradual progression intensifies when FLA is added into the model, aligning with the fact that TLR5 signaling is also IRAK 1 dependent (Seki et al., 2008), further reducing the amount of IRAK 1 available at a given moment. The model appeared to still be actively producing RNA beyond timestep 60,000 when LPS was high as well, indicating that the model was still actively working through the available agonist molecules after this longer period of time whereas runs incorporating lower agonist levels appeared to stabilize earlier, producing less RNA overall and generally being able to work through available agonist at a faster rate.

Experimental results did not align with the predicted cell activation generated through modeling. While the model had not shown any notable increase in cell activity with increases in LPS alone, increasing the concentration of LPS utilized in experimental BMDM stimulation from 0.05 μg/mL to 5.00 μg/mL significantly increased cellular IL-1β production. However, 0.05 and 0.50 μg/mL doses of LPS produced similar levels of IL-1β, which did align with model predictions. Incorporating FLA into experimental testing revealed that, generally speaking, the addition of FLA to cells stimulated with LPS did cause an increase in IL-1β production, as predicted by the model. However, there were discrepancies that arose when 0.50 μg/mL FLA was used for stimulation in combination with 0.50 μg/mL and 5.00 μg/mL LPS, with decreases in IL-1β production compared to samples stimulated with lower concentrations of FLA. This

may tie back to the aforementioned low TLR5 receptor expression level, and to the MYD88-independent pathway initiated by TLR4 that was not considered by the computational model. Unlike most TLR cascades, TLR4 operates via both MYD88-dependent and MYD88-independent mechanisms, with the independent pathway associated with IFN-I production (Yamamoto *et al.*, 2003) rather than pro-inflammatory cytokines like IL-1β (Gribar et al., 2008). When this pathway is considered, it seems plausible that the middle concentration of FLA may have pulled IRAK1 away from the TLR4 cascade for TLR5 signaling, leading the TLR4 signaling pathway to operate primarily via MYD88-independent mechanisms. This would then result in the production of more IFN-I over IL-1β, relative to cells stimulated with lower levels of FLA that would not need to rely on this secondary cascade. Increasing FLA ten-fold from this middle concentration to 5.00 μg/mL would lead the TLR5 pathway to be utilized more frequently. As the TLR5 pathway only operates by MYD88-dependent mechanisms that produce pro-inflammatory cytokines, the increased stimulation of this pathway would then increase the IL-1β production from that seen in cells stimulated with 0.50 μg/mL FLA, which aligns with experimental results. Though it was not tested, it would be reasonable to assume that this increase in FLA from 0.50 μg/mL to 5.00 μg/mL further increases IFN-I production as well as IL-1β production, as the TLR4 pathway will shift toward MYD88-independent mechanisms as IRAK1 is used more frequently in TLR5 signaling. Further studies should consider quantifying IFN-1 production via an ELISA, to test this hypothesis.

The model was unable to predict the trends observed with M1 polarization intensity, but it still seems likely that further modifications could be made to improve its value. IRAK1, NFκB, and TLR5 were unable to be adjusted directly to their RT-qPCR-indicated value, as this would have reduced their respective inputs to a value ≤ 1. Dropping to such a low input would prevent

the model from being able to complete both the TLR4 or TLR5 signaling cascades, as there would have been too few IRAK1, NFκB, and TLR5 molecules present for output to have been produced within the observed timeframe. These proteins serve as potential targets for future changes that may affect modeling results while maintaining model stability. Other unchanged values, such as those affecting component size and velocity, could be modified as well to better reflect differences in movement within BMDM compared to monocytes. Additionally, the model may benefit from the incorporation of the MYD88-independent TLR4 signaling pathway, as it is currently not considered (Liew et al., 2018) but is suspected to play a role in how BMDM respond to dual TLR4 and TLR5 stimulation. The decreased level of IRAK 1 in BMDM provides evidence that these cells could rely on this IRAK-independent pathway more frequently than the monocytes that provided the basis for the original model, and the inclusion of this secondary pathway may better reflect how TLR pathways operate in BMDM, alone and when stimulated simultaneously. There may also be value in the experimental testing of additional inflammatory cytokines, such as IL-12. The original model had been tested against four proteins, aligning with IL-1β and NFκB but not with TNF-α or IL-6 (Liew et al., 2022). As only four factors were tested, the study of others may reveal that the production of an alternative cytokine may better reflect modeling results. IL-12 has long been considered a strong candidate for tumor treatments, with debate on the best method of cytokine delivery (Nguyen et al., 2020). If the model-predicted cell activation aligned with IL-12 expression in stimulated BMDM, this information may provide further insight into the prediction of BMDM therapeutic efficacy and could promote the use of BMDM as a delivery method.

While the model was unable to be directly adapted for BMDM based on RT-qPCR results alone, I chose to continue with testing the therapeutic efficacy of stimulated BMDM to

investigate if M1 polarization intensity had any effect on therapeutic efficacy. Evidence that differences in TLR agonist concentration contribute to differences in the efficacy of BMDM as a tumor therapy would provide grounds that the model could be used in predicting a therapeutic response, once adjusted to better reflect TLR mechanisms in BMDM. For therapeutic testing, "low", "medium", and "high" treatments were determined based on the distinct levels of IL-1β produced by BMDM following dual TLR4 and TLR5 stimulation. Mice treated with BMDM activated at a high level initially showed a significant slowing of tumor growth compared to mice from the control group, but this difference appeared to wear off at approximately day 20, with tumor size suddenly spiking, leaving the growth rate and severity to match that of the control group for the remainder of the testing period. BMDM activated at a medium level displayed an initial benefit compared to the control when mice were injected with both BMDM and EMT6 simultaneously, but this effect wore off earlier than those at a high level. In both simultaneous and delayed BMDM injections, over the course of the 28-day measurement period mice from the medium treatment group displayed larger, more aggressive tumors, emphasizing that these BMDM were displaying M2 effects. BMDM activated at a low level initially did not contribute to any notable difference in tumor size compared to the control group, but over time their tumor growth rate seemed to stabilize, leading mice treated with these cells to develop smaller tumors and have an increased probability of survival compared to the control group.

As all treatments contributed to tumor sizes and survival probabilities that were different from those of the control group, it is clear that the concentrations of agonists used for TLR stimulation are critical in predicting the response of a tumor to BMDM-based therapeutic agents. The initial difference in tumor size observed in cells treated with BMDM activated at a high and low level may have been caused by IL-1β, which would have had a limited long-term effect due

to the role that the acidic pH of the TME would play in the generation of bioreactive IL-1β (Edye et al., 2015). TNF-α, which was produced by all cells at a similar level regardless of agonist concentration, is also rapidly degraded in acidic environments, and may not contribute to long-term benefits if cells are unable to maintain the M1 phenotype for an extended period of time following signaling from cytokines in the TME (Heming et al., 2001). Additionally, both IL-1β and TNF-α have been known to contribute to tumor progression if present in excess (Gelfo et al., 2020) (Wang et al., 2008), and this may have played a role in the sudden spikes in tumor growth rates seen in the high and medium treatment groups. However, from this alone, it is unclear why the BMDM activated at a medium level would have transitioned so quickly to serve in the long-term promotion of tumor growth and severity. To better understand the differences observed between these groups, and to provide insight into the mechanisms that contribute to the sustained benefit provided by BMDM activated with low LPS and FLA levels, studying the production of additional cytokines following TLR stimulation could be beneficial. If pro-inflammatory cytokines that had not been previously studied were shown to have differences in production rates with changes in concentrations of TLR agonists used for stimulation, some of the inconsistencies that currently exist when comparing activation intensity and therapeutic efficacy could be resolved. Again, IL-12 should be considered a cytokine of interest, as IL-12 has been known to persist even in acidic conditions (Chen et al., 2023).

Another plausible distinction between the treatment groups may relate to differences between the standard MYD88-dependent TLR4 pathway and the aforementioned MYD88-independent pathway. Some proteins involved with the independent pathway, such as IFN-I, may affect tumor development. Weak, chronic IFN-I responses, for example, are known to contribute to tumor cell survival through the development of resistance to DNA damage, while

more intense responses are known to be cytotoxic (Cheon et al., 2023). The BMDM activated at a medium level may have produced just enough IFN-I to produce a weak response, which could have generated DNA damage relatively quickly to cause the sharp spike in tumor size and severity seen around day 14. BMDM activated at a high level may have initially produced levels of IFN-I that were cytotoxic, but as BMDM began to transition into an M2 phenotype in response to TME signaling, the production of IFN-I may have dropped to a lower dose, promoting the DNA damage seen earlier on with the medium treatment group and causing a increase in tumor growth rate. This would provide an explanation for the similarities between the final tumor sizes and probability of survival in mice treated with BMDM activated at high and low levels. As BMDM stimulated with lower agonist concentrations may have been able to operate without the use of the MYD88-independent pathway, they would lack the IFN-I response that cells activated at medium and high levels would generate, which may explain why BMDM activated at a low level were more likely to show a sustained anti-tumor effect than BMDM activated at a medium level.

Adapting the computational model through RT-qPCR may have proved to be unsuccessful, but the differences in tests of the therapeutic capabilities of cells stimulated with varying TLR agonist concentrations highlight the potential use of an accurate model of the BMDM response to TLR4 and TLR5 stimulation in the prediction of the therapeutic efficacy of BMDM as a treatment for tumors. Through the consideration of alternative output variables over IL-1β, the continued adjustment of parameters, and the inclusion of the MYD88-independent pathway, one may be able to generate a model similar to the THP-1 model that could be used to predict how TLR signaling in macrophages may be harnessed to slow or reduce tumor size and severity. Further experimental testing of cytokines may reveal more information about how

BMDM are responding to TLR stimulation, and how the MYD88-independent TLR4 pathway may contribute to delayed pro-tumor effects in cells treated with LPS. Expanding upon therapeutic testing, the further delay of the BMDM injection from day 7 to day 14 would provide insight into the therapeutic efficacy of BMDM in treating more established, aggressive tumors, as day 7 tumors are still relatively small and controlled. Additionally, repeated injections of BMDM at days 7, 14, and 21, or at days 14 and 21, would better replicate the repeated treatments that are common in cancer therapies, and would test whether the injection of fresh BMDM into the tumor site allows cells to retain M1 characteristics for an extended period of time, allowing highly-activated cells to better control tumor size without loss of efficacy.

References

Anderson, N. R., Minutolo, N. G., Gill, S., & Klichinsky, M. (2021). Macrophage-Based Approaches for Cancer Immunotherapy. *Cancer research*, *81*(5), 1201–1208. https://doi.org/10.1158/0008-5472.CAN-20-2990

Andreesen, R., Scheibenbogen, C., Brugger, W., Krause, S., Meerpohl, H. G., Leser, H. G., Engler, H., & Löhr, G. W. (1990). Adoptive transfer of tumor cytotoxic macrophages generated in vitro from circulating blood monocytes: a new approach to cancer immunotherapy. *Cancer research*, *50*(23), 7450–7456.

Anaya, J. M., Shoenfeld, Y., Rojas-Villarraga, A., Levy, R. A., & Cervera, R. (Eds.). (2013). *Autoimmunity: From Bench to Bedside*. El Rosario University Press.

Chávez-Galán, L., Olleros, M. L., Vesin, D., & Garcia, I. (2015). Much More than M1 and M2 Macrophages, There are also CD169(+) and TCR(+) Macrophages. *Frontiers in immunology, 6*, 263. https://doi.org/10.3389/fimmu.2015.00263

Cheon, H., Wang, Y., Wightman, S. M., Jackson, M. W., & Stark, G. R. (2023). How cancer cells make and respond to interferon-I. *Trends in cancer, 9*(1), 83–92. https://doi.org/10.1016/j.trecan.2022.09.003

Chen, P., Yang, W., Nagaoka, K., Huang, G. L., Miyazaki, T., Hong, T., Li, S., Igarashi, K., Takeda, K., Kakimi, K., Kataoka, K., & Cabral, H. (2023). An IL-12-Based Nanocytokine Safely Potentiates Anticancer Immunity through Spatiotemporal Control of Inflammation to Eradicate Advanced Cold Tumors. *Advanced science (Weinheim, Baden-Wurttemberg, Germany), 10*(10), e2205139. https://doi.org/10.1002/advs.202205139

Edye, M. E., Brough, D., & Allan, S. M. (2015). Acid-dependent Interleukin-1 (IL-1) Cleavage Limits Available Pro-IL-1β for Caspase-1 Cleavage. *The Journal of biological chemistry, 290*(42), 25374–25381. https://doi.org/10.1074/jbc.M115.667162

Gribar, S. C., Richardson, W. M., Sodhi, C. P., & Hackam, D. J. (2008). No longer an innocent bystander: epithelial toll-like receptor signaling in the development of mucosal inflammation. *Molecular medicine (Cambridge, Mass.), 14*(9-10), 645–659. https://doi.org/10.2119/2008-00035.Gribar

Gu, L. C., Erdös, E. A., Chiang, H. S., Calderwood, T., Tsai, K., Visor, G. C., Duffy, J., Hsu, W. C., & Foster, L. C. (1991). Stability of interleukin 1 beta (IL-1 beta) in aqueous solution: analytical methods, kinetics, products, and solution formulation implications. *Pharmaceutical research, 8*(4), 485–490. https://doi.org/10.1023/a:1015851228163

Heming, T. A., Tuazon, D. M., Davé, S. K., Chopra, A. K., Peterson, J. W., & Bidani, A. (2001). Post-transcriptional effects of extracellular pH on tumor necrosis factor-alpha production in RAW 246.7 and J774 A.1 cells. *Clinical science (London, England : 1979), 100*(3), 259–266.

Jain, A., Kaczanowska, S., & Davila, E. (2014). IL-1 Receptor-Associated Kinase Signaling and Its Role in Inflammation, Cancer Progression, and Therapy Resistance. *Frontiers in immunology, 5*, 553. https://doi.org/10.3389/fimmu.2014.00553

Juhas, U., Ryba-Stanisławowska, M., Szargiej, P., & Myśliwska, J. (2015). Different pathways of macrophage activation and polarization. *Postepy higieny i medycyny doswiadczalnej (Online), 69*, 496–502. https://doi.org/10.5604/17322693.1150133

Kawai, T., Takeuchi, O., Fujita, T., Inoue, J., Mühlradt, P. F., Sato, S., Hoshino, K., & Akira, S. (2001). Lipopolysaccharide stimulates the MyD88-independent pathway and results in activation of IFN-regulatory factor 3 and the expression of a subset of lipopolysaccharide-inducible genes. *Journal of immunology (Baltimore, Md. : 1950), 167*(10), 5887–5894. https://doi.org/10.4049/jimmunol.167.10.5887

Kawasaki, T., & Kawai, T. (2014). Toll-like receptor signaling pathways. *Frontiers in immunology, 5*, 461. https://doi.org/10.3389/fimmu.2014.00461

Liew, C. W., Phuong, T., Jones, C. B., Evans, S., Hoot, J., Weedling, K., Ingram, D., Nganga, S., & Kurt, R. A. (2018). A computational approach to unraveling TLR signaling in murine mammary carcinoma. *Computers in biology and medicine, 93*, 56–65. https://doi.org/10.1016/j.compbiomed.2017.12.013

Liew, C.W., Polanco, L., Manalang, K., & Kurt, R.A. (2022). An experimental and computational approach to unraveling interconnected TLR signaling cascades. *Informatics in Medicine Unlocked, 30*. https://doi.org/10.1016/j.imu.2022.100939

Martinez, F. O., & Gordon, S. (2014). The M1 and M2 paradigm of macrophage activation: time for reassessment. *F1000prime reports, 6*, 13. https://doi.org/10.12703/P6-13

Nguyen, K. G., Vrabel, M. R., Mantooth, S. M., Hopkins, J. J., Wagner, E. S., Gabaldon, T. A., & Zaharoff, D. A. (2020). Localized Interleukin-12 for Cancer Immunotherapy. *Frontiers in immunology, 11*, 575597. https://doi.org/10.3389/fimmu.2020.575597

Pan, Y., Yu, Y., Wang, X., & Zhang, T. (2020). Tumor-Associated Macrophages in Tumor Immunity. Frontiers in immunology, 11, 583084. https://doi.org/10.3389/fimmu.2020.583084

Pennini, M. E., Perkins, D. J., Salazar, A. M., Lipsky, M., & Vogel, S. N. (2013). Complete dependence on IRAK4 kinase activity in TLR2, but not TLR4, signaling pathways underlies decreased cytokine production and increased susceptibility to Streptococcus pneumoniae infection in IRAK4 kinase-inactive mice. *Journal of immunology (Baltimore, Md. : 1950), 190*(1), 307–316. https://doi.org/10.4049/jimmunol.1201644

Rébé, C., & Ghiringhelli, F. (2020). Interleukin-1β and Cancer. *Cancers, 12*(7), 1791. https://doi.org/10.3390/cancers12071791

Seki, E., & Brenner, D. A. (2008). Toll-like receptors and adaptor molecules in liver disease: update. Hepatology (Baltimore, Md.), 48(1), 322–335. https://doi.org/10.1002/hep.22306

Seledtsov, V. I., Goncharov, A. G., & Seledtsova, G. V. (2015). Clinically feasible approaches to potentiating cancer cell-based immunotherapies. *Human vaccines & immunotherapeutics, 11*(4), 851–869. https://doi.org/10.1080/21645515.2015.1009814

van Dalen, F. J., van Stevendaal, M., Fennemann, F. L., Verdoes, M., & Ilina, O. (2018). Molecular Repolarisation of Tumour-Associated Macrophages. *Molecules (Basel, Switzerland), 24*(1), 9. https://doi.org/10.3390/molecules24010009

Wynn, T. A., Chawla, A., & Pollard, J. W. (2013). Macrophage biology in development, homeostasis and disease. *Nature, 496*(7446), 445–455. https://doi.org/10.1038/nature12034

Wang, X., & Lin, Y. (2008). Tumor necrosis factor and cancer, buddies or foes?. *Acta pharmacologica Sinica, 29*(11), 1275–1288. https://doi.org/10.1111/j.1745-7254.2008.00889.x

Xu, S., Xiong, Y., Fu, B., Guo, D., Sha, Z., Lin, X., & Wu, H. (2023). Bacteria and macrophages in the tumor microenvironment. *Frontiers in microbiology, 14*, 1115556. https://doi.org/10.3389/fmicb.2023.1115556

Yamamoto, M., Sato, S., Hemmi, H., Hoshino, K., Kaisho, T., Sanjo, H., Takeuchi, O., Sugiyama, M., Okabe, M., Takeda, K., & Akira, S. (2003). Role of adaptor TRIF in the MyD88-independent toll-like receptor signaling pathway. *Science (New York, N.Y.), 301*(5633), 640–643. https://doi.org/10.1126/science.1087262

Yunna, C., Mengru, H., Lei, W., & Weidong, C. (2020). Macrophage M1/M2 polarization. *European journal of pharmacology, 877*, 173090. https://doi.org/10.1016/j.ejphar.2020.173090

Zheng, X. F., Hong, Y. X., Feng, G. J., Zhang, G. F., Rogers, H., Lewis, M. A., Williams, D. W., Xia, Z. F., Song, B., & Wei, X. Q. (2013). Lipopolysaccharide-induced M2 to M1 macrophage transformation for IL-12p70 production is blocked by Candida albicans mediated up-regulation of EBI3 expression. *PloS one, 8*(5), e63967. https://doi.org/10.1371/journal.pone.0063967

Figures

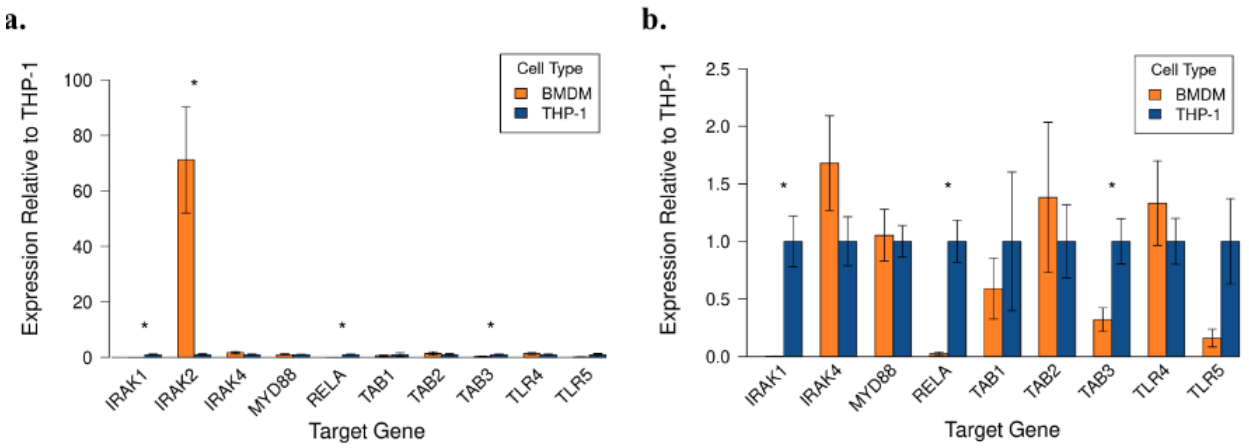

Figure 1. Differences in TLR-Associated Gene Expression. RT-qPCR results showing expression of all ten tested TLR-related genes, set against the expression levels in THP-1 cells (a). IRAK2 excluded to allow visualization of expression differences in the nine other TLR-related genes (b). Asterisks represent significance at a level of $p < 0.05$ (*). The data represent the average ∓ SE of three separate experiments.

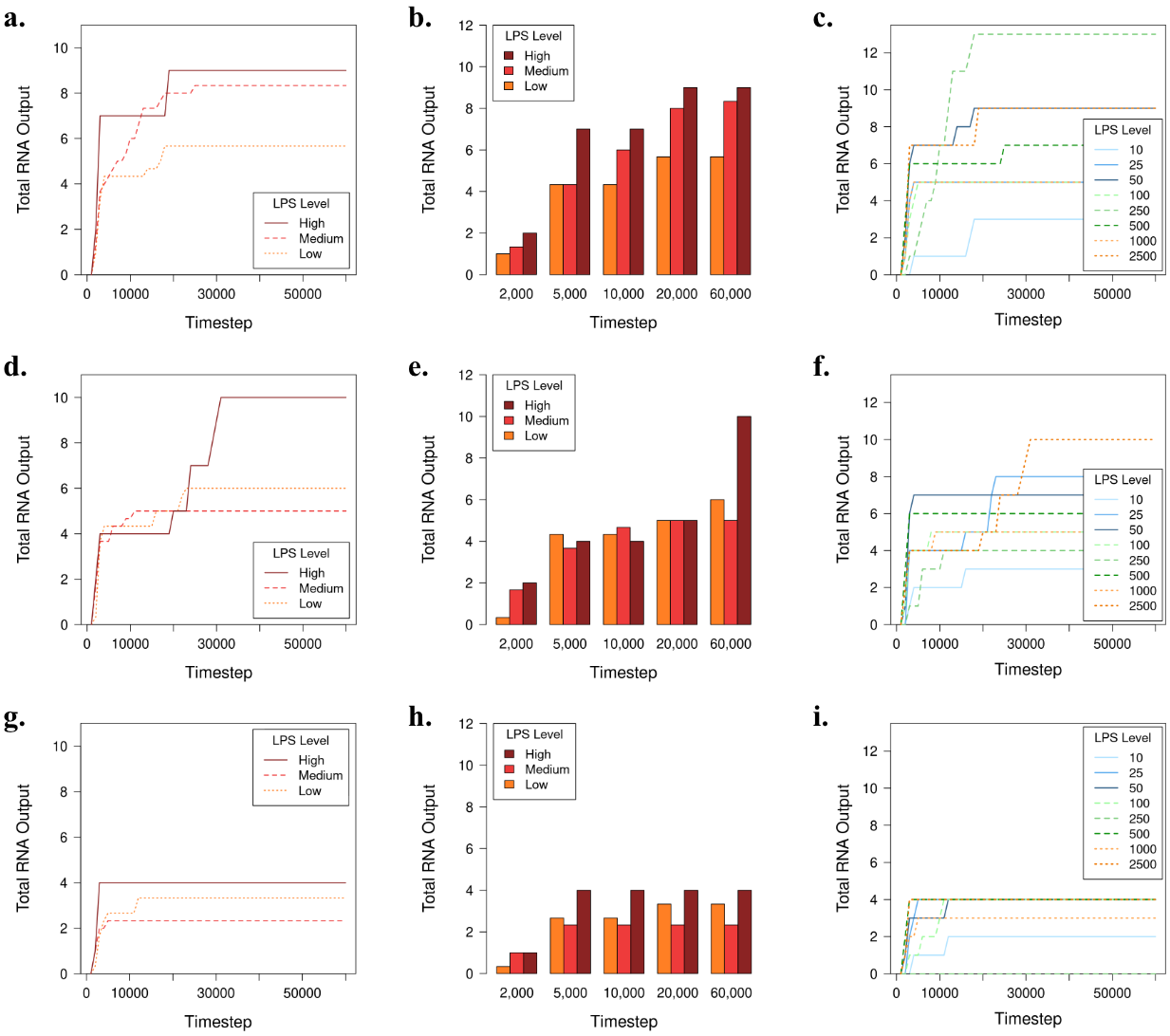

Figure 2. **Prediction of RNA Output with TLR4 Stimulation From Models 1-3.** Line charts displaying the cumulative RNA output overtime for model 1 (a), model 2 (d) and model 3 (g), with runs grouped into high, medium, and low doses of LPS. Clustered bar charts visualizing the RNA output with LPS variation overtime for grouped data from model 1 (b), model 2 (e) and model 3 (h). Line charts representing the cumulative RNA output overtime for individual LPS level data for model 1 (c), model 2 (f) and model 3 (i). Runs grouped as "low" are shown as blue solid lines, those grouped as "medium" are shown as green dashed lines, and those grouped as "high" are shown as orange dotted lines.

a.

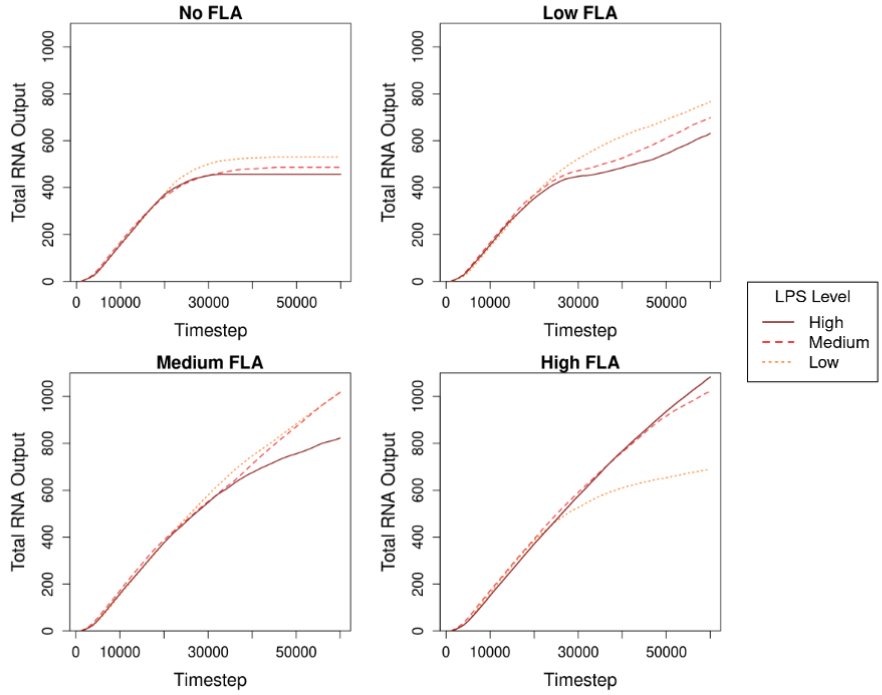
No FLA
Low FLA
Medium FLA
High FLA
Total RNA Output
Timestep
0
200
400
600
800
1000
0
10000
30000
50000
LPS Level
High
Medium
Low

b.

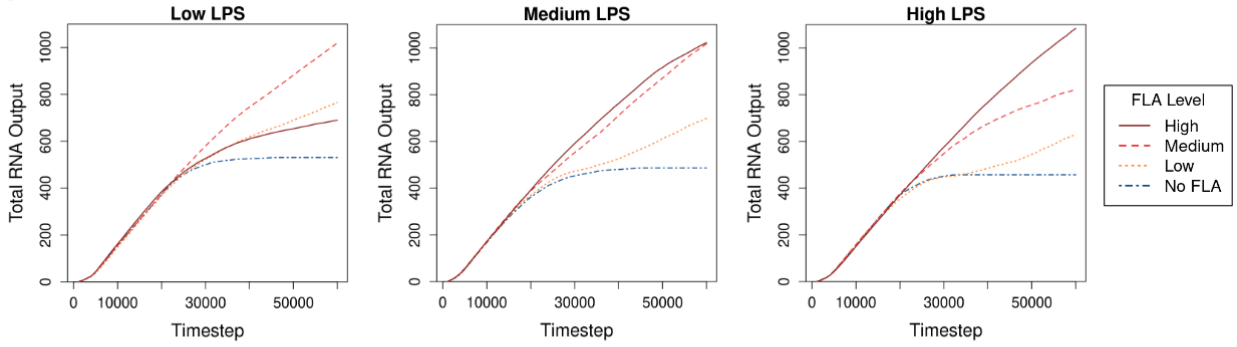
Low LPS
Medium LPS
High LPS
Total RNA Output
Timestep
0
200
400
600
800
1000
0
10000
30000
50000
FLA Level
High
Medium
Low
No FLA

c.

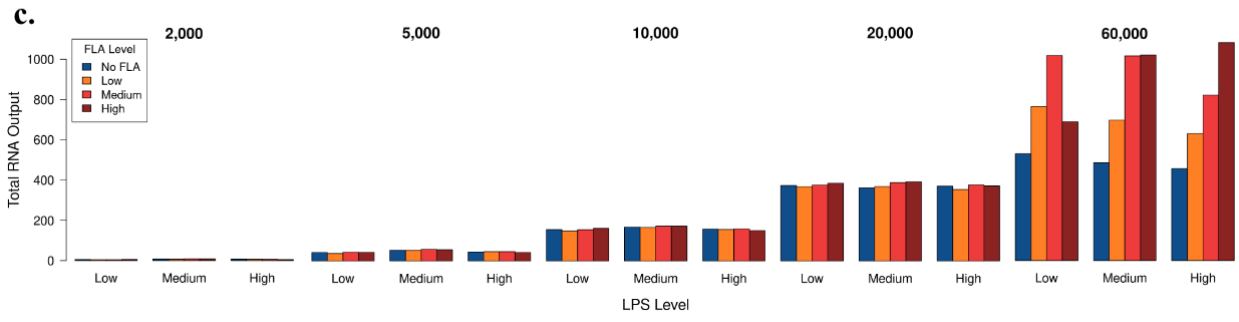
2,000
5,000
10,000
20,000
60,000
FLA Level
No FLA
Low
Medium
High
Total RNA Output
0
200
400
600
800
1000
Low
Medium
High
LPS Level

d.

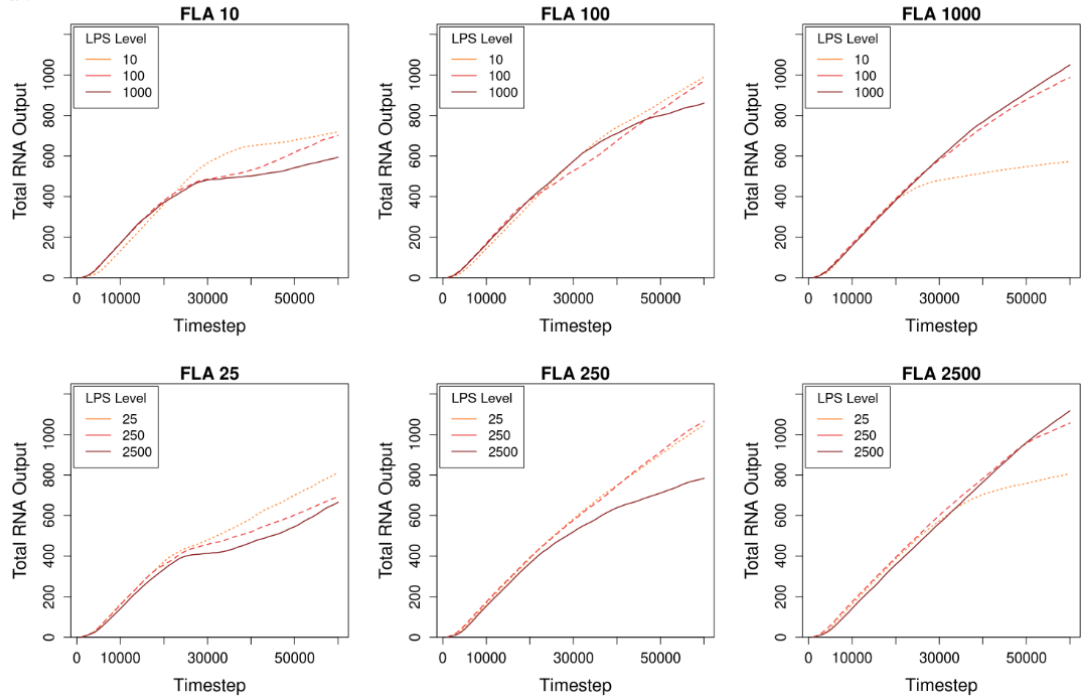

Figure 3. **Prediction of RNA Output with TLR4 and TLR5 Stimulation From Model 4.** Line charts of RNA output with changes in grouped LPS level, divided according to grouped FLA level (a). Line charts of RNA output with changes in FLA level, divided according to LPS level (b). Bar plots depicting the intertwined relationship of LPS and FLA adjustments over time, with timestep shown in bold above each set of three bars (c). Line charts of RNA output with changes in individual LPS levels, divided by individual FLA levels (d).

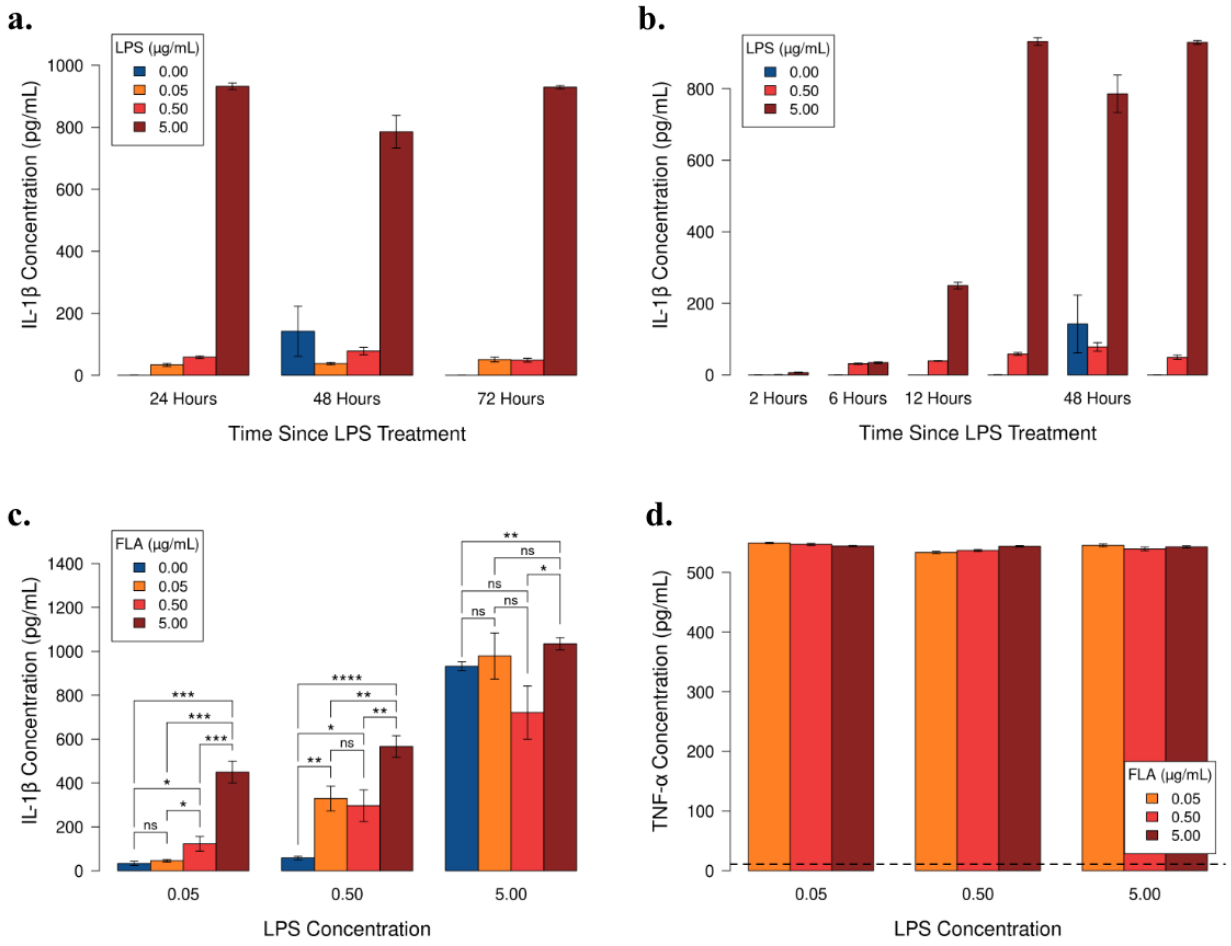

Figure 4. Inflammatory Cytokines Produced by TLR-stimulated BMDM Concentrations of IL-1β in supernatants of BMDM 24, 48, and 72 hours post-stimulation with 1 of 3 LPS concentrations or HBSS as a control (a). Concentrations of IL-1β in supernatants of BMDM 2, 6, 12, 24, 48, and 72 hours post-stimulation with 1 of 3 LPS concentrations (b). Concentrations of IL-1β in supernatants of BMDM 24 post-stimulation with 1 of 3 LPS concentrations alone or in combination with 1 of 3 FLA concentrations (c). Concentrations of TNF-α in supernatants of BMDM 24 post-stimulation with 1 of 3 LPS concentrations alone or in combination with 1 of 3 FLA concentrations. Dashed line represents the average TNF-α concentration in the supernatants of BMDM treated with HBSS alone(d). All data represent the average ∓ SE of three separate experiments. Asterisks represent significance at levels of 95% confidence (*), 99% confidence (**), and 99.9% confidence (***).

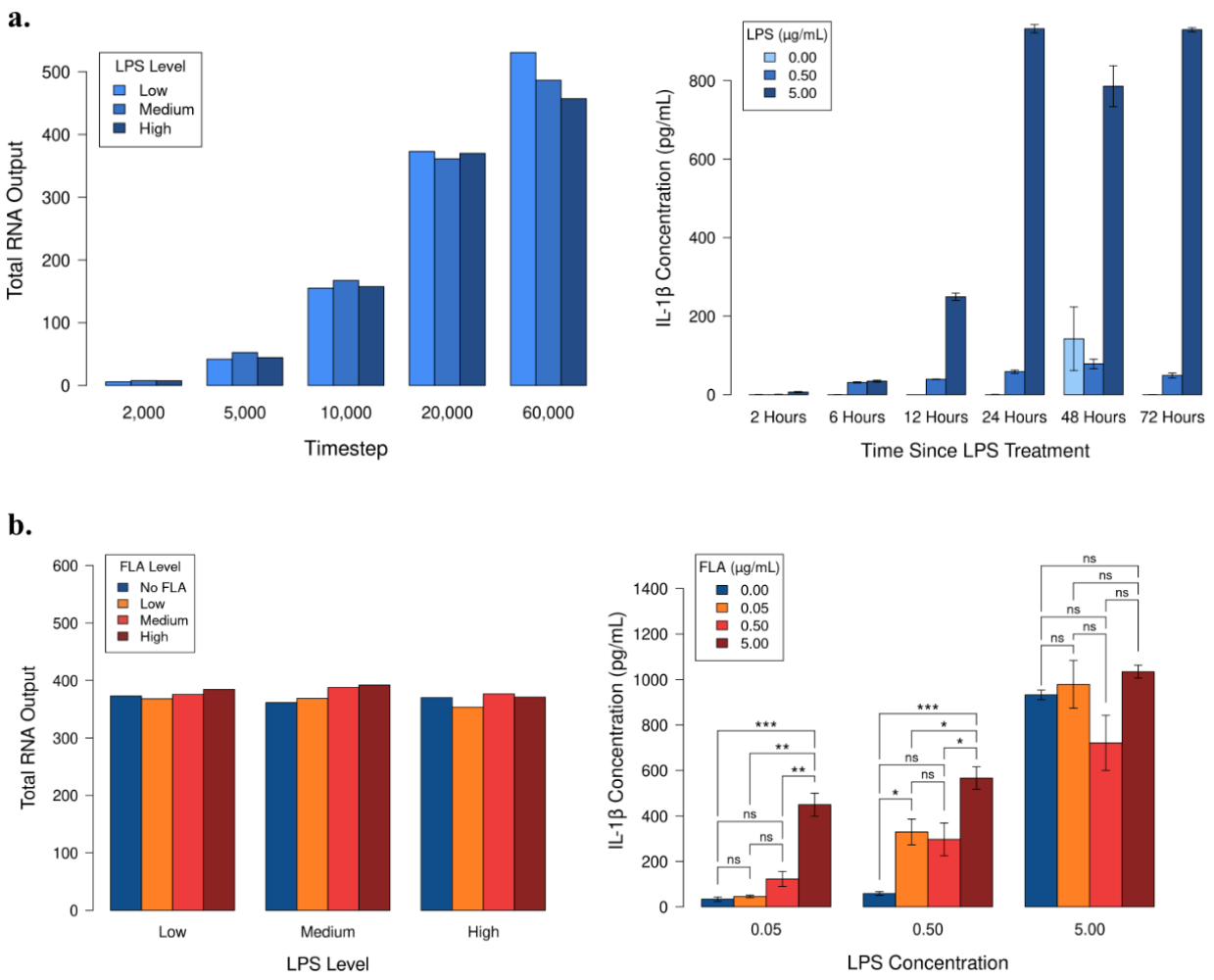

Figure 5. Inconsistencies between modeled and experimental results. Side-by-side comparisons of model-generated RNA outputs, shown on the left, and experimentally calculated IL-1β production, shown on the right, when cells are stimulated with LPS alone overtime (a) and when cells are stimulated with LPS and FLA simultaneously and collected 24 hours-post stimulation, or at the estimated modeling equivalent of timestep 20,000 (b). All experimental data represent the average ∓ SE of three separate experiments. Asterisks represent significance at levels of 95% confidence (*), 99% confidence (**), and 99.9% confidence (***).

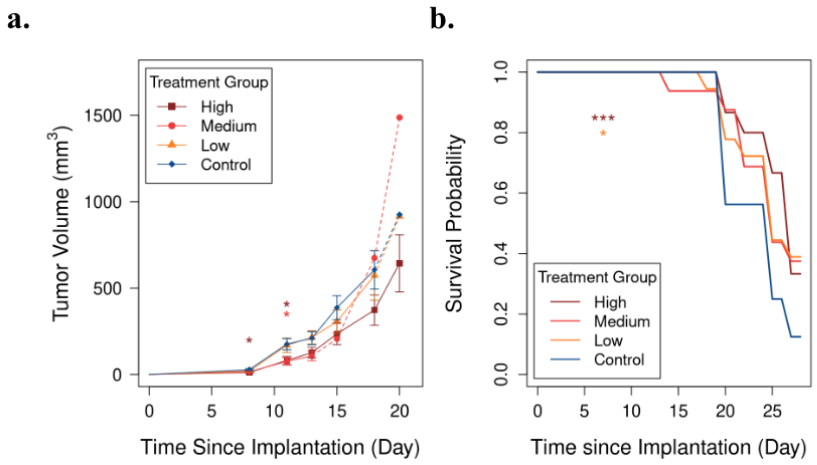

Figure 6. Simultaneous Injection of EMT6 and BMDM. Line chart showing the average size of EMT6-derived tumors in mice that received a simultaneous injection of BMDM stimulated with 5.00 µg/mL LPS and 5.00 µg/mL FLA ("High" treatment group), 0.50 µg/mL LPS and 0.50 µg/mL FLA ("Medium" treatment group), 0.05 µg/mL LPS and 0.05 µg/mL FLA ("Low" treatment group), or HBSS ("Control" treatment group) (a). Dashed lines indicate data generated by exponential regression rather than data collected experimentally. The data represent the average ∓ SE of three separate experiments, each with a sample size of 4-6 mice per treatment. Kaplan meier curves showing survival probability overtime (b). Asterisks represent significance at levels of 95% confidence (*) and 99.9% confidence (***).

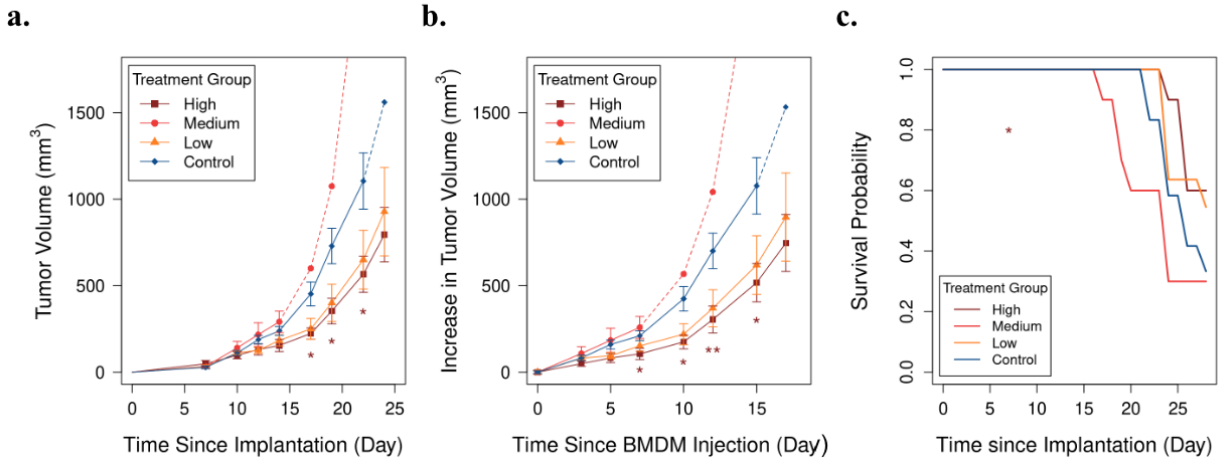

Figure 7. Delayed injection of BMDM. Line chart of the average tumor volume of mice that received an injection of BMDM stimulated with 5.00 µg/mL LPS and 5.00 µg/mL FLA ("High" treatment group), 0.50 µg/mL LPS and 0.50 µg/mL FLA ("Medium" treatment group), 0.05 µg/mL LPS and 0.05 µg/mL FLA ("Low" treatment group), or HBSS ("Control" treatment group) one week following EMT6 injection (a). Line chart displaying the change in tumor volume from a given treatment's average tumor volume at day 7 (b). Dashed lines indicate data generated by exponential regression rather than data collected experimentally. The data represent the average ∓ SE of two separate experiments, each with a sample size of 4-6 mice per treatment group. Kaplan meier curves showing survival probability overtime (c). Asterisks represent significance at levels of 95% confidence (*) and 99% confidence (**).

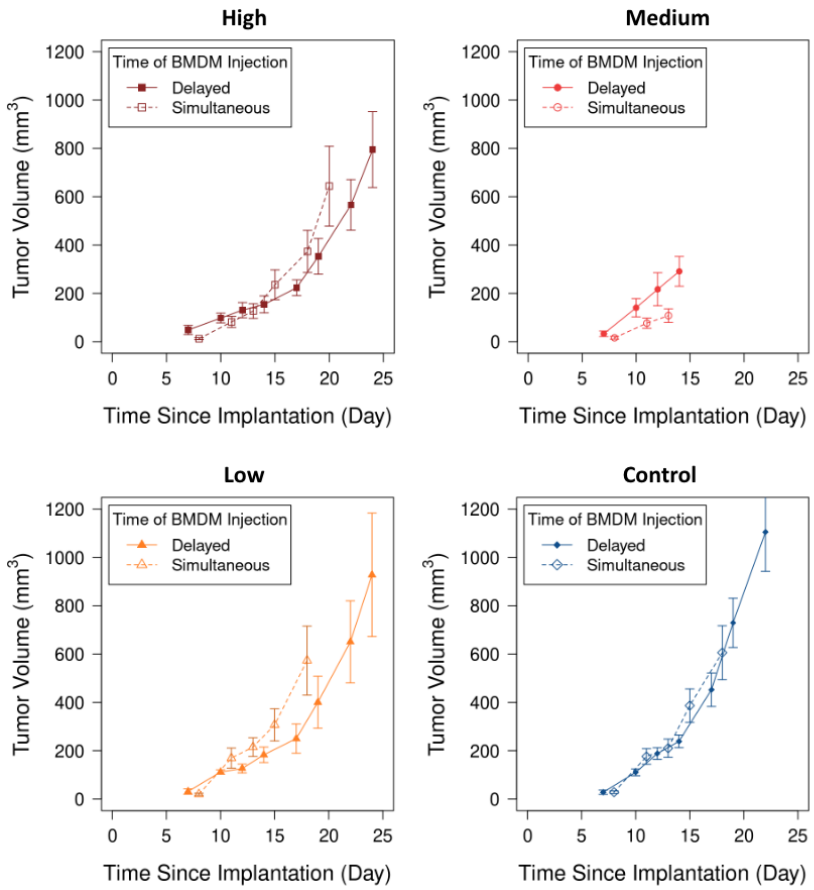

Figure 8. Comparison of Simultaneous and Delayed BMDM Injection. Line charts of the average tumor volume of mice that received an injection of BMDM stimulated with 5.00 µg/mL LPS and 5.00 µg/mL FLA ("High" treatment group), 0.50 µg/mL LPS and 0.50 µg/mL FLA ("Medium" treatment group), 0.05 µg/mL LPS and 0.05 µg/mL FLA ("Low" treatment group), or HBSS ("Control" treatment group), either one week following EMT6 injection or simultaneously with the EMT6 injection. The data represent the average of three separate simultaneous experiments and two separate delayed experiments, each with a sample size of 4-6 mice per treatment group.

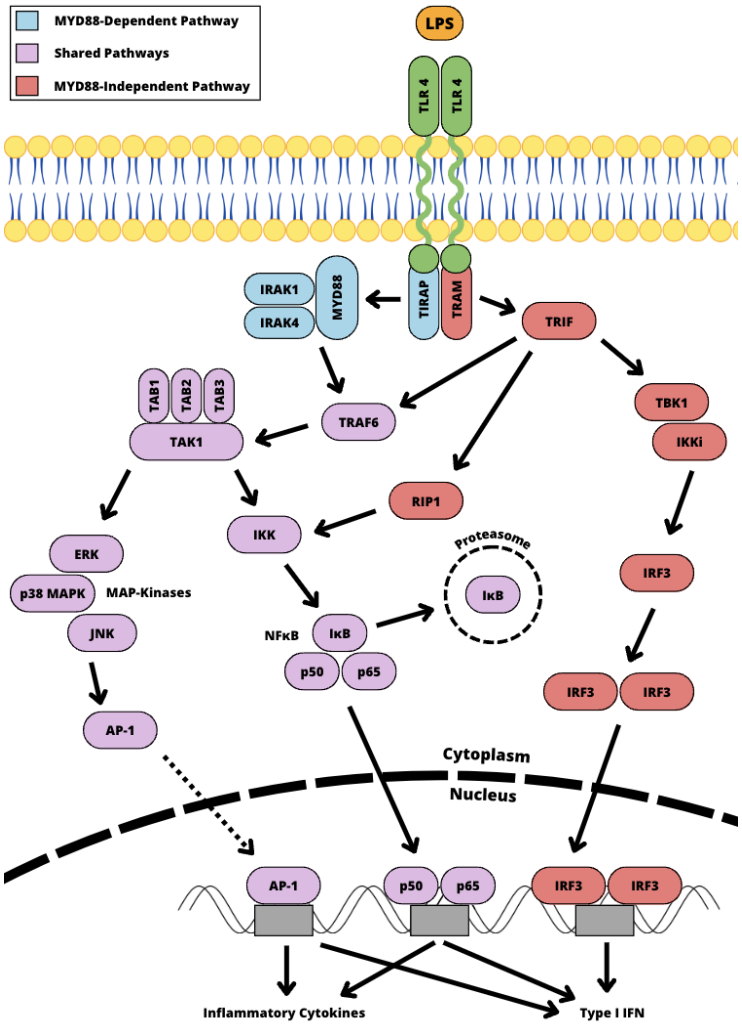

Figure 9. TLR4 Signaling Pathways. LPS recognition by the TLR4 receptor initiates MYD88-independent (red) or MYD88-dependent (blue) signaling through TRAM or TIRAP, which go on to produce inflammatory cytokines and/or type 1 interferons.

Tables

Table 1. Model Parameter Adjustments

		IRAK1	IRAK2	IRAK4	MYD88	RELA	TAB1	TAB2	TAB3	TLR4	TLR5
BMDM : THP-1 Expression Ratio		0.00235	71.17885	1.67956	1.05215	0.02308	0.59037	1.38139	0.31919	1.33234	0.16041
THP-1 Modeling Input Value		100	100	50	250	50	50	50	50	25	25
BMDM Modeling Input Value	**Model 1**	25	100	50	250	50	50	100	25	25	5
	Model 2	30	100	50	250	50	50	100	25	25	5
	Model 3	25	100	50	250	50	50	50	25	25	5
	Model 4	27	500	121	211	50	91	191	21	27	10

Table 2. Mathematical Modeling of Tumor Sizes

Experiment	Treatment	Equation	Adj. R Squared	P-Value
Simultaneous	Medium	ln(y) = -0.59295 + 0.39488*x	0.2836	2.87e-04
Simultaneous	Low	ln(y) = 0.54648 + 0.31364*x	0.4280	2.18e-12
Simultaneous	Control	ln(y) = 1.37678 + 0.27270*x	0.4644	1.885e-12
Delayed	Medium	ln(y) = 1.44601 + 0.29124*x	0.3683	3.211e-05
Delayed	Control	ln(y) = 2.76985 + 0.19096*x	0.7626	< 2.2e-16

Table 3. Assumptions of Computational Model Construction & Adaptation

Concept	Description	Assumption(s) Made
Component Movement	How each component moves & changes that occur when interacting with other components in the modeled 3D space.	Component movement & interaction is unaffected by the relative abundance of any individual component, or by the relative location of a component within the extracellular space, cell membrane, intermembrane space, or nucleus.
Reversion Time	Components remain in their "changed" state, following interaction with a different component, before reverting to their original state.	All components are able to revert back to their original state from their changed state. The length of time that components remain in their changed state before reversion is consistent.
Decay Time	Components produced following interaction between components last before decaying.	All components produced from interaction decay. The length of time that produced components last before decaying is consistent.
Cell Type	How TLR signaling proceeds in cells of varying types.	BMDM and THP-1 respond to LPS and FLA in the similar manners, with signaling operating via the same pathway in each cell type.
TLR Pathway Components	The particular proteins included within the modeled signaling pathways.	Of the proteins affiliated with TLR4/TLR5 signaling, 24 are primarily responsible for pathway completion. TLR4 signaling operates via MYD88-dependent mechanisms only.
Pathway Inclusion	The particular signaling pathways included in the computational model.	Signaling via the TLR4 and TLR5 pathways alone can describe general trends in pro-inflammatory cell activation.

Table 4. Assumptions of Modeling Analysis

Concept	Description	Assumption(s) Made
RNA Output	RNA transcribed from activated NFκB-mediated transcription of the CCL2 gene is analyzed as a modeling output value of interest.	RNA produced by NFκB-mediated transcription directly results in the production of pro-inflammatory cytokines. Cumulative levels of RNA overtime align with experimentally produced levels of IL-1β.
Timestep Correspondence	The estimated relationship between modeled timesteps and real-world time points, estimated from analysis of prior modeling data.	Timestep 60,000 aligns approximately with 72 hours.